PASJ: Publ. Astron. Soc. Japan , 1–??,
© 2010. Astronomical Society of Japan.

arXiv:0908.1460v2 [astro-ph.IM] 18 Jan 2010

FAST: A Fully Asynchronous Split Time-Integrator for Self-Gravitating Fluid

Takayuki R.Saitoh[1] and Junichiro Makino[1,2,3]

[1] *Division of Theoretical Astronomy, National Astronomical Observatory of Japan, 2–21–1 Osawa, Mitaka-shi, Tokyo 181–8588.*

[2] *Center for Computational Astrophysics, National Astronomical Observatory of Japan, 2–21–1 Osawa, Mitaka-shi, Tokyo 181–8588*

[3] *Department of Astronomical Science, School of Physical Sciences, The Graduate University for Advanced Studies (SOKENDAI), 2–21–1 Osawa, Mitaka-shi, Tokyo 181–8588, Japan.*

saitoh.takayuki@nao.ac.jp,saitoh.takayuki@cfca.jp

(Received 2009 August 10; accepted 2010 January 13)

Abstract

We describe a new algorithm for the integration of self-gravitating fluid systems using SPH method. We split the Hamiltonian of a self-gravitating fluid system to the gravitational potential and others (kinetic and internal energies) and use different time-steps for their integrations. The time integration is done in the way similar to that used in the mixed variable or multiple stepsize symplectic schemes. We performed three test calculations. One was the spherical collapse and the other was an explosion. We also performed a realistic test, in which the initial model was taken from a simulation of merging galaxies. In all test calculations, we found that the number of time-steps for gravitational interaction were reduced by nearly an order of magnitude when we adopted our integration method. In the case of the realistic test, in which the dark matter potential dominates the total system, the total calculation time was significantly reduced. Simulation results were almost the same with those of simulations with the ordinary individual time-step method. Our new method achieves good performance without sacrificing the accuracy of the time integration.

Key words: galaxies:starburst — galaxies:ISM — ISM:structure — method:numerical

1. Introduction

The number of particles used in simulations of galaxy formation with N-body/Smoothed Particle Hydrodynamics (SPH) method has not increased much since the early days of Katz & Gunn (1991) and Navarro & Benz (1991), though the number of particles used in pure N-body cosmological simulations has increased drastically. For N-body simulations, the largest run in 1991 used $\sim 2 \times 10^6$ particles (Suto & Suginohara 1991) and the largest run recently performed used $\sim 7 \times 10^{10}$ particles (Kim et al. 2009). The number of particles has grown by nearly four orders of magnitudes in two decades. On the other hand, for N-body/SPH simulations of galaxy formation, the first simulations used ~ 4000 SPH particles for a single halo (Katz & Gunn 1991) and the largest simulation which is performed recently used $\sim 3.2 \times 10^5$ SPH particles for a single halo (Governato et al. 2009). [1] The scale up factor is only 80 in two decades. This is because time-steps become quite short in dense and compact self-gravitating gas clouds of star-forming regions.

This problem is severer in simulations with higher resolution, since these simulations resolve denser gas. In general, supernova (SN) explosion in dense regions leads the shortest time-step. Here we roughly estimate the decrease of the time-steps due to SNe. We consider a compact region of the interstellar medium (ISM) with the temperature of $T_{\rm ISM}$, where the sound speed is $c_{\rm ISM}$, as a potential site of the star formation and that the region is rapidly heated to $T_{\rm SN}$, where the sound speed is $c_{\rm SN}$, by SN with the energy of $E_{\rm SN}$. The contraction factor between the time-step of the ISM after the SN, $dt_{\rm SN}$, and before the SN, $dt_{\rm ISM}$, in the compact region is

$$\begin{aligned} dt_{\rm SN}/dt_{\rm ISM} &= c_{\rm ISM}/c_{\rm SN}, \\ &\propto (T_{\rm ISM}/T_{\rm SN})^{1/2}, \\ &\propto {E_{\rm SN}}^{-1/2}\ m^{1/2}\ {T_{\rm ISM}}^{1/2}, \end{aligned} \tag{1}$$

where $E_{\rm SN}$ is the energy of the single SN and m is the mass of the heated region or the mass resolution in Lagrange schemes such as SPH, respectively, and we use $T_{\rm SN} \propto E_{\rm SN}/m$. From this equation, we can easily find that the contraction factor becomes smaller when (i) mass resolution becomes higher and (ii) the temperature of the ISM becomes lower (see also section 2 for more detailed discussion). Thus high-resolution simulations which model the ISM with low temperature ($< 10^4$ K) require much shorter time-steps than conventional simulations of galaxy formation with a cooling cut off at $\sim 10^4$ K.

The individual time-step method (Aarseth 1963;

[1] Note that a part of SPH particles were converted into star particles, thus the number of SPH particles was reduced during the galaxy evolution.

McMillan 1986; Makino 1991a) reduces the total calculation cost significantly in simulations which cover a wide range of timescales, by assigning different time-steps to different particles and integrating only a small fraction of particles with small time-steps. Here, we extend this idea for the time integration of self-gravitating fluid particles in order to achieve a further reduction of the total calculation cost. Our new method allows an individual fluid particle to have different time-steps for gravitational and hydrodynamical interactions and integrates these interactions asynchronously. As stated earlier, the smallest time-steps are associated with particles heated by SNe feedback. These particles have the thermal and kinetic energy many orders of magnitudes larger than the gravitational potential energy. Therefore, if we assign different time-steps to gravitational and hydrodynamical forces, we should be able to use much longer time-step for gravity, thereby accelerating simulations by a large factor. We named this time-integration scheme for self-gravitating fluid as FAST (**F**ully **A**synchronous **S**plit **T**ime-integrator).

There are two main advantages of the FAST method over the traditional individual time-step method for self-gravitating fluid simulations. First, FAST reduces unnecessary gravitational force evaluations in small time-steps induced by SNe. Since the number of dark matter and stellar particles is usually larger than that of SPH particles in typical simulations of galaxy formation, the calculation cost of gravity is larger than that of hydrodynamics. This reduction of unnecessary evaluation of gravity is quite efficient for the acceleration of simulations. Simulations with hardware accelerators, such as GRAPEs (Sugimoto et al. 1990; Ito et al. 1991; Okumura et al. 1993; Makino et al. 1997; Kawai et al. 2000; Makino et al. 2003), receive further benefit from FAST, since hardware accelerators are inefficient in calculations with small number of particles, because of small bandwidth and large latency of the bus between the host computer and the accelerator. The second advantage appears when we combine the individual time-steps and the tree method (Barnes & Hut 1986). Since the cost of the tree construction is independent of the number of active particles, it dominates the total calculation cost when the number of particles with small time-steps is small. Consequently, the total performance of simulation is not much improved by the use of individual time-steps. Table 1 of Wadsley et al. (2004) showed such a bad case. We can see that a half of the cost of smallest steps is that of the "Tree building" part. By adopting FAST, the number of tree construction is reduced and hence simulations with the individual time-step and tree methods are accelerated significantly.

There are several other ways to reduce the cost of simulations with the individual time-steps and tree methods. McMillan & Aarseth (1993) applied the local update to the tree structure around particles which were updated, instead of reconstructing the whole tree structure at each step. This technique was used in `GADGET-1/2` (Springel et al. 2001; Springel 2005). In `VINE` (Wetzstein et al. 2009; Nelson et al. 2009), the construction frequency of tree structure was reduced by skipping several continuous time-steps and reusing old tree structure for force calculation. They updated the tree structure at every ~ 10 steps for the problem they showed in their paper. FAST method can be combined with these schemes to further reduce the cost of tree construction, if necessary.

Our approach is similar to the multiple time-step method used in molecular dynamics, in which the long-range Coulomb force is updated less frequently than short-range van del Waals force (Streett et al. 1978). The main difference is that we combine the force splitting with individual time-steps.

The structure of this paper is as follows. In section 2, we estimate and compare the time-steps of particles in the hot region of star-forming galaxies. In section 3, we describe our new integration method for self-gravitating fluid, FAST. We briefly explain its implementation in §4. We present the results of test calculations and timing results in section 5. A discussion on the maximum acceleration factor by FAST appears in section 6. In section 7, we provide summary.

2. Estimate of Time-steps in Heated Regions of Star Forming Galaxies

In this section, we estimate typical time-steps of an SPH particle in star forming regions of actively star forming galaxies in N-body/SPH simulations of galaxy formation. This estimation allows us to estimate the maximum gain in the performance due to the use of the FAST scheme. We compare the typical Courant time-step of an SPH particle heated by SNe with the typical gravitational time-step of the particle.

Here we estimate the typical Courant time-step of an SPH particle heated by SNe. For simplicity, we adopt following four assumptions. First, we adopt a single stellar population (SSP) approximation for a star particle with Salpeter initial mass function (IMF) (Salpeter 1955) and the range of this IMF is set to be 0.1 $M_\odot$ to 100 $M_\odot$. For this IMF, the specific SN rate is $\epsilon_{\rm SN} \simeq 0.0074$ SN/M$_\odot$, where we assume 8 $M_\odot$ or heavier stars become SNe at the final phase of their evolutions. Second, we assume that each SN injects the thermal energy of $E_{\rm SN} = 10^{51}$ ergs to the surrounding ISM (the nearest $N_{\rm NB}$ particles). Third, we assume that the whole energy from SNe in a star particle discharges in a single event (this is one of SN feedback implementations proposed by Okamoto et al. 2008). Finally, we assume that the masses of the stellar and gas particles are the same.

The mean additional internal energy for $N_{\rm NB}$ SPH particles due to SNe of a single stellar particle is given by

$$\begin{aligned} U_{\rm SN} &= \frac{\epsilon_{\rm SN} m_* E_{\rm SN}}{N_{\rm NB} m_{\rm SPH}}, \\ &\simeq 0.0074 \times 10^{51} \times \frac{m_*}{N_{\rm NB} m_{\rm SPH}} \ [\text{ergs M}_\odot{}^{-1}], \\ &\simeq \frac{3.7 \times 10^{15}}{N_{\rm NB}} [\text{ergs g}^{-1}], \end{aligned} \tag{2}$$

where m_* and $m_{\rm SPH}$ are the masses of stellar and gas particles, respectively, and we use the relation $m_* = m_{\rm SPH}$.

The sound speed, $c_{\rm SN}$, of the heated gas region is

$$c_{\rm SN} \simeq \sqrt{\gamma(\gamma-1)U_{\rm SN}}, \simeq \frac{6.4\times10^2}{{N_{\rm NB}}^{1/2}}\ [{\rm km\ s^{-1}}], \quad (3)$$

where we assume an ideal gas with the adiabatic index of $\gamma = 5/3$. The original internal energy of the ISM before SNe, $U_{\rm ISM}$, is quite small, therefore we neglected $U_{\rm ISM}$ in the estimation of $c_{\rm SN}$. The corresponding temperature of the heated region is $T_{\rm SN} \sim 3.2\times10^6\ (N_{\rm NB}/32)^{-1/2}$ [K]. Note that this temperature implies very short cooling timescale of $\sim 10^3$ yr. In real star-forming region, initially the SN ejecta have much high temperature, and the cooling time is much longer. In order to model SN feedback in a physically correct way, therefore, some tricks which prevent the quick radiative cooling (Gerritsen 1997; Thacker & Couchman 2000; Stinson et al. 2006) is necessary. We here assume some of these tricks are used. The size of an SPH particle, λ, is

$$\lambda = \Big(\frac{3}{4\pi}\frac{m_{\rm SPH}}{\rho}\Big)^{1/3}, \quad (4)$$

where ρ is the density of the SPH particle. Combining equations (3) and (4), we obtain the sound crossing time, $t_{\rm SN} \equiv \lambda/c_{\rm SN}$, in the heated region as follows:

$$t_{\rm SN} \simeq 4\times10^4\Big(\frac{m_{\rm SPH}}{1000\ M_\odot}\Big)^{1/3}\Big(\frac{100\ {\rm cm^{-3}}}{N_{\rm H}}\Big)^{1/3}[{\rm yr}], \quad (5)$$

where we adopt $N_{\rm NB} = 32$ and $N_{\rm H}$ is the hydrogen number density of the heated region. The typical Courant time-step in the region is $dt_{\rm SN} \sim 0.1\times t_{\rm SN}$. This equation tells us that the smallest time-step in simulations involving the low temperature ISM and SNe becomes shorter when mass resolution becomes higher and injected region becomes denser.

By comparing equation (3) with the typical velocity of the ambient ISM, we can obtain the contraction factor of the time-steps caused by a SN explosion. Although the typical temperature of giant molecular clouds (GMCs) is low (~ 10 K) and the corresponding sound speed in GMCs is small (~ 0.2 km s^{-1}), the linewidth of GMCs is higher than that expected by the sound speed of the ISM and predicts that GMCs are supported by supersonic turbulence. Thus we use empirical relations for the estimate of the timescale, instead of the local sound speed. The linewidth-size relation, which is often referred as Larson's law (Larson 1981; Solomon et al. 1987; Heyer & Brunt 2004), gives us the typical velocity at the size of cloud. Larson's law is as follows:

$$\sigma_{\rm c} \simeq \Big(\frac{L_{\rm c}}{1\ {\rm pc}}\Big)^{1/2}\ [{\rm km\ s^{-1}}], \quad (6)$$

where $\sigma_{\rm c}$ and $L_{\rm c}$ are the linewidth and size of a cloud, respectively, and the applicable range of this relation is $0.1\ {\rm pc} \le L_{\rm c} \le 100\ {\rm pc}$. Combining the virial theorem and this relation, we obtain cloud mass-linewidth relation (Solomon et al. 1987) that

$$M_{\rm c} = 2000\Big(\frac{\sigma_{\rm c}}{1\ {\rm km\ s^{-1}}}\Big)^4\ M_\odot, \quad (7)$$

where $M_{\rm c}$ is a cloud mass. When we substitute $N_{\rm NB}m_{\rm SPH}$ into $M_{\rm c}$, we obtain the mass resolution-linewidth relation:

$$\sigma_{\rm c} = \Big(\frac{N_{\rm NB}m_{\rm SPH}}{2000\ M_\odot}\Big)^{1/4}\ [{\rm km\ s^{-1}}]. \quad (8)$$

This equation leads the velocity of the smallest cloud which can be expressed with the resolution of the simulation. The contraction factor of the time-step in the ISM by a SN explosion, $f_{\rm cont}$, is

$$f_{\rm cont} \equiv \frac{\sigma_{\rm c}}{c_{\rm SN}}, = \Big(\frac{N_{\rm NB}m_{\rm SPH}}{2000\ M_\odot}\Big)^{1/4}\Big(\frac{6.4\times10^2}{{N_{\rm NB}}^{1/2}}\Big)^{-1}, \sim 1.8\times10^{-2}\Big(\frac{m_{\rm SPH}}{1000\ M_\odot}\Big)^{1/4}, \quad (9)$$

where we adopted $N_{\rm NB} = 32$. This equation clearly shows that the Courant condition becomes quite tight in ISM heated by a SN explosion. When we use 6 km s^{-1}, which is the sound speed of the ISM at 10^4 K, as the typical velocity of the ISM, the contraction factor is $f_{\rm cont} \sim 5.3\times10^{-2}$. We again adopted $N_{\rm NB} = 32$. The contraction factor for simulations with the multiphase ISM and turbulence motions is smaller than that in conventional simulations of galaxy formation with a cooling cut off at 10^4 K.

In conventional simulations of galaxy formation, where the typical mass resolution is $10^6\ M_\odot$ and the highest density of the ISM is 0.1 cm^{-3}, the typical time-step for the heated region is $dt_{\rm SN} \sim 4\times10^5$ yr. The typical gravitational time-step, one-tenth of the local free-fall time at 0.1 cm^{-3}, is 5×10^6 yr. The difference between the Courant and gravity time-steps is ~ 10. On the other hand, in state-of-the-art simulations involving the multiphase ISM, where $m_{\rm SPH} = 10^3\ M_\odot$ and $N_{\rm H} = 100$ cm^{-3}, the typical time-step is $dt_{\rm SN} \sim 4\times10^3$ yr, whereas the the typical gravitational time-step at 100 cm^{-3} is 1.6×10^5 yr. The difference between two time-steps is ~ 40 and this difference is larger than that in conventional simulations. These simple estimates tell us that FAST can reduce gravity steps by a factor of $10-40$. FAST is more efficient in simulations with high resolution.

Thanks to the rapid increase of the computational power and the advance of numerical techniques, the mass resolution in current high resolution simulations of the galactic scale ISM has been quite high ($\sim 1000\ M_\odot$). It will be soon reach the point than the mass resolution at where the number of SN events in an SSP particle is less than unity. [2] In such simulations, SN events are necessary to be treated as not an association of SNe in every SSP particle but discrete events in a fraction of SSP particles so that the global SN event rate is consistent with the adopted IMF. Otherwise, we would introduce "fractional" SNe, which clearly would give wrong results for SNe feedback. By this modification in the treatment of SNe, the

[2] When an SSP particle mass is lower than a critical mass $m_{\rm c}$, which is obtained by $\epsilon_{\rm SN}m_{\rm c} = 1$, the number of SNe events in an SSP particle is lower than unity. If we use $\epsilon_{\rm SN} = 0.0074$, $m_{\rm c} \sim 135\ M_\odot$.

sound speed of the ISM in heated regions becomes much higher than that in equation (3) and the crossing time in these regions becomes much shorter than that in equation (5). We show here a simple estimate of time-steps in the case where SN explosions are discrete events in SSP particles. When we consider a SN explosion takes place in discrete manner, the received energy of the surrounding ISM of a compact region is modified as follows:

$$\begin{aligned} U_{\rm SN,d} &= \frac{E_{\rm SN}}{N_{\rm NB} m_{\rm SPH}}, \\ &\simeq \frac{10^{51}}{N_{\rm NB} m_{\rm SPH}} \ [\text{ergs M}_\odot{}^{-1}], \\ &\simeq \frac{5.0\times10^{17}}{N_{\rm NB}} \Big(\frac{1\ M_\odot}{m_{\rm SPH}}\Big) \ [\text{ergs g}^{-1}], \end{aligned} \tag{10}$$

where we again neglected the original internal energy because the value is sufficiently low compared with this value. The sound speed of the hot region is

$$\begin{aligned} c_{\rm SN,d} &= \sqrt{\gamma(\gamma-1)U_{\rm SN,d}}, \\ &\simeq \frac{7.5\times10^{3}}{{N_{\rm NB}}^{1/2}} \Big(\frac{1\ M_\odot}{m_{\rm SPH}}\Big)^{1/2} \ [\text{km s}^{-1}]. \end{aligned} \tag{11}$$

The contraction factor is

$$\begin{aligned} f_{\rm cont} &= \Big(\frac{N_{\rm NB} m_{\rm SPH}}{2000\ M_\odot}\Big)^{1/4} \Big\{\frac{7.5\times10^{3}}{{N_{\rm NB}}^{1/2}} \Big(\frac{1\ M_\odot}{m_{\rm SPH}}\Big)^{1/2}\Big\}^{-1}, \\ &\simeq 2.7\times10^{-4}\Big(\frac{m_{\rm SPH}}{1\ M_\odot}\Big)^{3/4}. \end{aligned} \tag{12}$$

Note that the mass dependency in this equation is much stronger than that in equation (9). Combining equations (11) and (4), the sound crossing time in the heated region, $t_{\rm SN,d}$, is

$$t_{\rm SN,d} \simeq 3.3\times10^{2}\Big(\frac{m_{\rm SPH}}{1\ M_\odot}\Big)^{5/6} \Big(\frac{100\ \text{cm}^{-3}}{N_{\rm H}}\Big)^{1/3} \ [\text{yr}], \tag{13}$$

where we adopt $N_{\rm NB} = 32$. We find that the mass resolution dependence in the equation (13) is stronger than that in the equation (5). Thus high resolution simulations of near future will be much harder than those of present. For efficient simulations, we have to introduce efficient numerical techniques which can handle a very wide range of time-steps. We believe that our new scheme will play an important role not only in current simulations but also in new simulations of galaxy formation in the near future.

3. Basic Idea

The basic idea of our new scheme is as follows. We allow gas (SPH) particles to have different time-steps for gravitational and hydrodynamical integrations. Thus, we extend the idea of individual time-steps, which allows different particles to have different time-steps, to allow single particle to have different time-steps for different interactions. We then asynchronously integrate gravity and hydrodynamics with these different time-steps. This is the essence of our FAST method. Since the problem we have to solve is the time-integration of very hot gas particles formed by SNe, we allow time-steps for gravity to be longer than those for hydrodynamics. To allow different time-steps for gravity and hydrodynamics, we use the technique of constructing multi-timestep symplectic integrator. We divide the Hamiltonian of a self-gravitating fluid system into a gravitational potential term and others, and integrate each part with its own time-step.

The Hamiltonian of a self-gravitating fluid system of N gas particles is expressed as

$$H = \sum_i^N \frac{p_i^2}{2m_i} + U(\boldsymbol{q},\boldsymbol{\rho},\boldsymbol{s}) - \sum_i^N \frac{G m_i m_j}{q_{ij}}, \tag{14}$$

where p_i and q_i are conjugate variables of the canonical equation for particle i, m_i is the mass of particle i, U is the internal energy of fluid, which is a function of $\boldsymbol{q}$, density, $\boldsymbol{\rho}$, and entropy, $\boldsymbol{s}$. Here, $\boldsymbol{q}$, $\boldsymbol{\rho}$, and $\boldsymbol{s}$ denote $(q_1,q_2,q_3,\ldots,q_N)$, $(\rho_1,\rho_2,\rho_3,\ldots,\rho_N)$, and $(s_1,s_2,s_3,\ldots,s_N)$, respectively. Since we take into account arbitrary forms of hydrodynamical interactions, we express the internal energy for fluid as $U(\boldsymbol{q},\boldsymbol{\rho},\boldsymbol{s})$. The first, second, and third terms in the right hand side of equation (14) are the kinetic, internal, and gravitational potential energy of the system, respectively. The actual equations for p and s contain the contributions of non-conservative terms like artificial viscosity and radiative cooling/heating. For simplicity, we here regard the system as adiabatic (i.e., s_i are treated as constants). Hence the internal energy term becomes the function of $(\boldsymbol{q},\boldsymbol{\rho})$ and can be regarded as a potential term in the Hamiltonian.

We split the Hamiltonian into the gravitational potential term and others (see appendix 1):

$$H_{\rm hydro} = \sum_i^N \frac{p_i^2}{2m_i} + U(\boldsymbol{q},\boldsymbol{\rho}), \tag{15}$$

$$H_{\rm grav} = -\sum_i^N \frac{G m_i m_j}{q_{ij}}. \tag{16}$$

We then obtain the following expression of a symplectic integrator with the second-order accuracy,

$$f(t+\Delta t) \approx e^{\frac{\Delta t}{2}\{,H_{\rm grav}\}} e^{\Delta t\{,H_{\rm hydro}\}} e^{\frac{\Delta t}{2}\{,H_{\rm grav}\}} f(t), \tag{17}$$

where "{ , }" is a Poisson bracket and Δt is a time-step. The equation (17) can schematically rewrite as follows:

$$v_0' = v_0 + \frac{1}{2}\Delta t\ a_{\rm grav}, \tag{18}$$

$$x_0 \rightarrow (\text{Hydro update}) \rightarrow x_1, \tag{19}$$

$$v_0' \rightarrow (\text{Hydro update}) \rightarrow v_1', \tag{20}$$

$$v_1 = v_1' + \frac{1}{2}\Delta t\ a_{\rm grav}, \tag{21}$$

where x, v, v', and $a_{\rm grav}$ indicate the position, the velocity, the half-step advanced velocity, and the acceleration of gravitational force, respectively. Subscripts 0 and 1 indicate epochs of time-integration at t and $t+\Delta t$, respectively.

There are many ways to integrate the hydrodynamical part of equation (17), we here choose the second-order symplectic method (e.g., Hernquist & Katz 1989). We divide equation (15) again into the following two parts:

$$H_{\rm hydro,T} = \sum_i^N \frac{p_i^2}{2m_i}, \tag{22}$$

$$H_{\rm hydro,U} = U(\boldsymbol{q}, \boldsymbol{\rho}). \tag{23}$$

Consider the case that $\Delta t_{\rm g} = l\Delta t_{\rm h}$, where l is a natural number. We obtain a new expression of equation (17) as

$$f(t+\Delta t) \approx e^{\frac{\Delta t_g}{2}\{,H_{\rm grav}\}} [e^{\frac{\Delta t_h}{2}\{,H_{\rm hydro,U}\}} e^{\Delta t_h\{,H_{\rm hydro,T}\}} e^{\frac{\Delta t_h}{2}\{,H_{\rm hydro,U}\}}]^l e^{\frac{\Delta t_g}{2}\{,H_{\rm grav}\}} f(t). \tag{24}$$

This equation tells us that we can reduce the computational cost of gravity if $\Delta t_g > \Delta t_h$ ($l > 1$). If we adopt $l = 1$, the integrator is the same as the standard "leap-frog" method for self-gravitating fluid.

In figure 1, we show schematic pictures of the usual leap-frog and FAST methods. For FAST, we consider the case that $dt_{\rm grav} = 2\ dt_{\rm hydro}$. The computational cost of gravitational force in FAST becomes half of the leap-frog method in this case. In practice, the time-step ratio, l, adaptively changes.

It should be noted that, even though we borrowed the formalism of symplectic integrators to describe our FAST method, the FAST method itself is not symplectic. This is because we change the time-steps for gravitational and hydrodynamical interactions, after we split the Hamiltonian. In addition, we use different time-steps for different particles. However, this issue is not as crucial as that is for pure N-body simulations, since the usual hydrodynamical simulations introduce a dissipation term. The time-integration of hydrodynamic simulations is usually time irreversible and is breaking the symplectic nature inherently.

There have been several proposed methods which can retain either symplecticness (Farr & Bertschinger 2007) or time symmetry (Makino et al. 2006) when used with the individual time-step method. However, these schemes are computationally expensive and it is not clear if the use of these schemes is worthwhile or not. In this paper, we concentrate on the traditional, non-symplectic implementation of individual time-step algorithm and its extension.

4. Implementation

4.1. The Code

The code used in this paper is a parallel tree SPH code, `ASURA`, which utilizes the special purpose hardware GRAPE (Saitoh in prep.). Gravitational force was solved by Tree with GRAPE (Makino 1991b). In this paper, we used the Phantom GRAPE library for calculations of gravity, which is a software emulator of GRAPE pipelines (kindly provided by Kohji Yoshikawa). We used an opening angle of 0.5 and only monopole moments for force calculations. Hydrodynamics was followed by the standard SPH method (e.g., Lucy 1977; Gingold & Monaghan 1977; Monaghan 1992). We used the "gather" formulation of SPH for the density estimation, whereas the "gather and scatter" formulation of SPH for the pressure gradient and the time derivation of internal energy (Monaghan 1992). We adopted the asymmetric form energy equation (e.g., Steinmetz & Mueller 1993). We iteratively determined the kernel radius of each SPH particle in every step in order to keep the number of neighbor particles, 32 ± 2. We used an artificial viscosity term, of which form is the same as that proposed by Monaghan (1997), in order to handle shocks. The value of the viscosity parameter, α, was set to be unity. `ASURA` adopts the variable and individual time-step method (McMillan 1986; Hernquist & Katz 1989). Following Makino (1991a), `ASURA` adopts an extended version of the individual time-step method, *i.e.*, the "hierarchical" time-step method where time-steps are quantized by the power of two of a baseline time-step in order to improve the simulation performance with individual time-steps. We also implemented the time-step limiter for hydrodynamical interactions in order to maintain the difference of time-steps among neighbor particles small enough (Saitoh & Makino 2009). Here we adopted the factor of the time-step difference in neighbors, $f = 4$. The current version of `ASURA` implements two time integrators, namely the ordinary leap-frog and FAST methods.

4.2. Time-steps

The time-steps were determined as follows. The gravity time-step of an i-th particle was estimated by

$$dt_{{\rm grav},i} = C_{\rm grav} \min\Big(\sqrt{\frac{\epsilon}{|\boldsymbol{a}_{{\rm grav},i}|}}, \frac{|\boldsymbol{a}_{{\rm grav},i}|}{|\dot{\boldsymbol{a}}_{{\rm grav},i}|}\Big), \tag{25}$$

where ϵ is a gravitational softening length, $C_{\rm grav}$ is a parameter which controls the accuracy (we here adopt 0.1), and $\dot{\boldsymbol{a}}_{{\rm grav},i}$ is the time derivation of the acceleration, respectively.

Following Monaghan (1997), the hydrodynamical time-step of the i-th SPH particle was determined by

$$dt_{{\rm hydro},i} = C_{\rm hydro} \frac{2h_i}{v_{{\rm sig},i}}, \tag{26}$$

where h_i is the kernel size of the SPH particle (the interaction scale is $2h_i$), $C_{\rm hydro} = 0.25$, and $v_{{\rm sig},i}$ is the local maximum signal-velocity of i-th particle defined by

$$v_{{\rm sig},i} = \max_j (c_i + c_j - 3w_{ij}), \tag{27}$$

where j indicates the indices of neighbor particles, c_i and c_j is the sound speed of i-th and j-th SPH particles and $w_{ij} = \boldsymbol{v}_{ij} \cdot \boldsymbol{x}_{ij}/|\boldsymbol{x}_{ij}|$ is a projected relative velocity between the SPH particles. We set $w_{ij} = 0$ if $w_{ij} > 0$.

When we use the FAST method, we asynchronously integrate gravity and hydrodynamics by the leap-frog method with different time-steps for gravity (Eq. 25) and hydrodynamics (Eq. 26). If $dt_{\rm grav} \neq 2^n dt_{\rm hydro}$ where n is an integer number of ≥ 0, we change the gravitational time-step so that it satisfies the above criterion

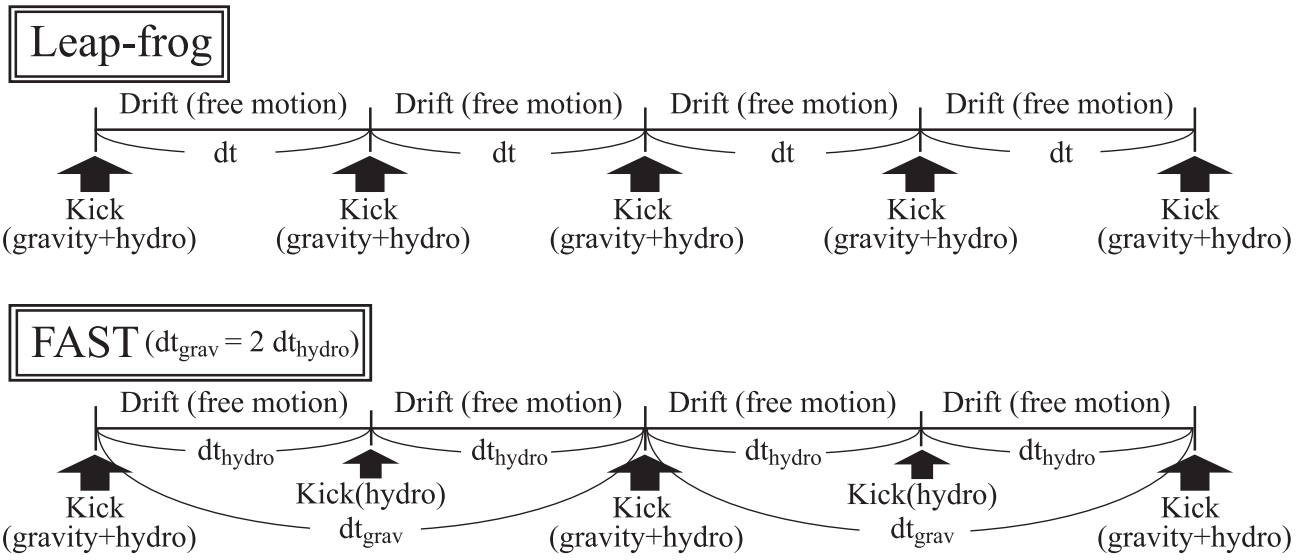

Fig. 1. The schematic picture of the leap-frog and FAST methods for the integration of a self-gravitating fluid. See also figure 1 in Fujii et al. (2007) for MVS and BRIDGE methods. "Kick" means the momentum exchanges between particles, while "Drift" denotes the free (inertial) motions under given velocity vectors.

in the following way: we reduce the time-step of gravity to $dt'_{\rm grav}$, where $dt_{\rm grav} \geq dt'_{\rm grav} = 2^n dt_{\rm hydro}$, and n is the maximum integer number that satisfies this relation. If $dt_{\rm grav} < dt_{\rm hydro}$, we reduce $dt_{\rm hydro}$ to the same value as $dt_{\rm grav}$.

When we used the ordinary leap-frog method, we picked up the smaller one of the two time-steps as the time-step of an SPH particle,

$$dt = \min(dt_{\rm grav}, dt_{\rm hydro}), \tag{28}$$

and synchronously integrated both gravity and hydrodynamics. In general, the acceleration and its differential terms in equation (25) should be measured relative to the total acceleration (*i.e.*, the sum of the gravitational and hydrodynamical accelerations). However, in the hydrodynamical simulations, the Courant condition leads the smaller time-step compared with the time-step obtained by the total acceleration. Therefore the simple determination by equation (28) worked sufficiently.

5. Numerical tests

We performed three tests. The first test was the collapse of a gas cloud and the second test was the point-like explosion of a self-gravitating gas cloud. The third test was a more realistic simulation. We performed simulations of galaxy-galaxy collisions, where galaxies consist of dark matter, star and gas particles. These tests incorporated both gravity and hydrodynamics and were representative of the evolution of self-gravitating fluid in galaxy formation simulation or other astrophysical simulations. We, hereafter, denote the results with the ordinary individual time-step method as "Ind" and the results with the individual time-step with the FAST method as "FAST", in tables and figures. The first two tests were designed as simple tests for the validity of the FAST method, while in the third test we investigated the actual gain in the calculation speed as well as the accuracy of the result.

The first and second tests were done on a system with a 2.4 GHz Opteron 280 processor (Italy core), while the third test was done on 2.2 GHz quad-core Opteron processors (Barcelona core) of Cray XT4 system at Center for Computational Astrophysics of National Astronomical Observatory of Japan. We used one CPU core for the first and second tests, whereas we used 128 CPU cores for the third test.

5.1. Test I: Three dimensional self-gravitational collapse tests

We performed the integration of three-dimensional spherical collapse of adiabatic gas (e.g., Evrard 1988; Hernquist & Katz 1989). This test is one of standard tests for SPH method which involves self-gravity.

We prepared a gas sphere with the total mass and the radius both unity. The gravitational constant was also set to be unity. The initial profile of the gas sphere was $\rho(r) \propto 1/r$, where r is the distance from the center of coordinates. The adiabatic index and the specific internal energy of the gas were set to be $\gamma = 5/3$ and 0.05, respectively. The gas sphere had a negative value of the total energy, $E \sim -0.6$. When the evolution starts, the sphere begins to collapse. The shock takes place in the central region and it propagates outward. Finally, the system reaches the state of virial equilibrium. In this test, we used 30976 particles for the sphere and we followed the evolution of the gas sphere to $T = 3$. We adopted 0.038 for the gravitational softening length.

Figure 2 shows radial profiles of density, pressure, and radial velocity in three different epochs, $T = 0.9$, 1.2 and 2.4, for both the ordinary individual time-step and FAST methods. In this figure, we plotted mean physical quantities of every 300 particles. It is obvious that the results of

two methods are identical. We also confirmed that these results agree well with the result obtained using global time-steps. Therefore we can conclude our new method is accurate enough.

Figure 3 shows the values of time-steps for gravity and hydrodynamics for the run with the FAST method as a function of the distance from the center at $T = 0.9$. Time-steps for gravity and hydrodynamics are different in the post-shock region and the same in the ambient, pre-shocked region. The transient region clearly matches with the shock front at the radius of ~ 0.2 (see the top-left panel of figure 2). The values of $dt_{\rm hydro}$ and $dt_{\rm grav}$ in the post-shock region differ by a factor up to four. Figure 4 shows cumulative fractions of $dt_{\rm hydro}$ and $dt_{\rm grav}$ for the simulation with the individual time-step with FAST. We can see that almost half of the particles have hydro time-steps smaller than the minimum time-step for the gravity.

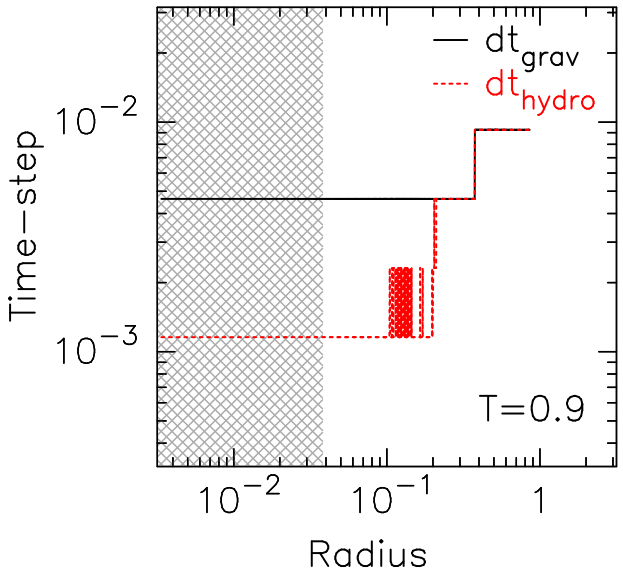

Fig. 3. Radial profiles of $dt_{\rm hydro}$ and $dt_{\rm grav}$ for the spherical collapse test with the individual time-step with FAST. The epoch is $T = 0.9$. Solid and dotted curves indicate $dt_{\rm grav}$ and $dt_{\rm hydro}$, respectively. The hatched region corresponds with the soften region for the particle at the center by the gravitational softening.

The errors of the total energy, the difference between the values of the total energy at the initial ($T = 0$) and final ($T = 3$) states, for the Ind and FAST methods are shown in table 1. $E_{\rm s}$ and $E_{\rm f}$ represent the initial ($T = 0$) total energy and the final ($T = 3$) total energy, respectively. These values are acceptably small. In our test runs, the absolute value of the energy error for the time integration with FAST is smaller than that for the time integration without FAST even though the time-step for gravity is larger. The errors caused by the gravitational and hydrodynamical integrations had the opposite signs and partially canceled each other.

In table 2, we show timing results of the collapse test. Our new method is faster than the original method, but not by a large factor. The calculation time of gravity is

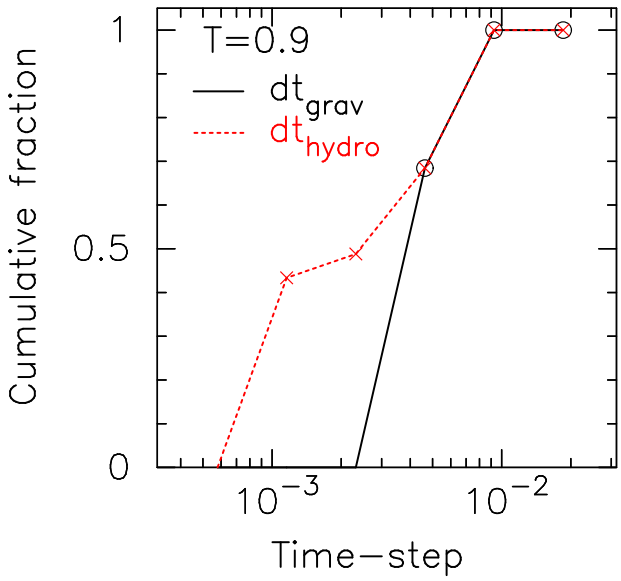

Fig. 4. Cumulative fractions of particles as a function of $dt_{\rm hydro}$ and $dt_{\rm grav}$ for the spherical collapse test with the individual time-step with FAST. The epoch is $T = 0.9$. Solid and dotted lines indicate cumulative fractions of $dt_{\rm grav}$ and $dt_{\rm hydro}$, respectively.

Table 1. Total energy errors for the spherical collapse test.

Method	$\lvert(E_{\rm s} - E_{\rm f})/E_{\rm s}\rvert$
Ind	3.0×10^{-3}
FAST	1.3×10^{-3}

reduced to two thirds, and that of tree construction is reduced to two fifths. However, in this test the hydrodynamics part dominates the total cost.

Table 3 shows the number of steps and integrated particles for the collapse test. The ordinary individual time-step method required 1979 steps for the simulation in our implementation. The FAST method required 2022 steps for the hydrodynamics part and 778 steps for the gravity part. The reduction of the calculation time for tree construction is directly proportional to the reduction of gravity steps. In our new method, the total number of integrated particles for the gravity part becomes almost two thirds of that for the hydrodynamics part in this test.

5.2. Test II: Three-dimensional explosion tests

Now, we discuss the result of three-dimensional explosion test. We designed this test to mimic an explosion of

Table 2. Timing results for the spherical collapse test.

	Time [sec]			
Method	Total	Gravity[a]	Hydro	Others
Ind	1754	682 (52)	960	112
FAST	1523	468 (20)	943	112

[a] The tree structure construction times in the gravity part are shown as parenthetical numbers.

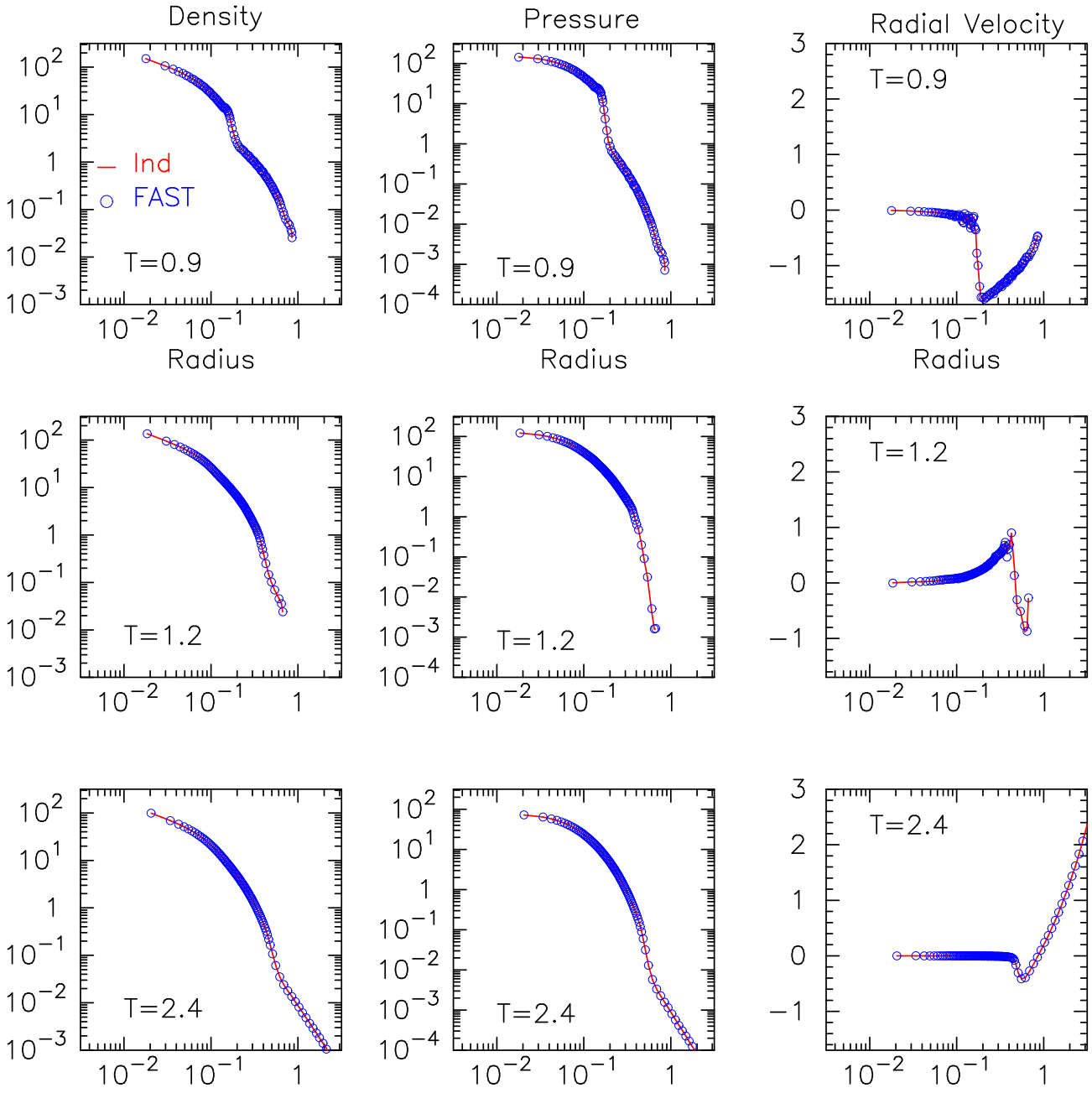

Fig. 2. Radial profiles of density (left), pressure (mid), and radial velocity (right) at $T = 0.9$, 1.2, and 2.4 (top to bottom). Horizontal axis is the distance from the origin of coordinates. Curves and circles indicate the profiles obtained with the individual and synchronous time-steps for gravity and hydrodynamics, "Ind", and the individual and asynchronous time-steps for gravity and hydrodynamics, "FAST".

Table 3. Steps and number of integrated particles for the spherical collapse test.

	Gravity		Hydro	
Method	steps	$N_{\rm int,grav}$	steps	$N_{\rm int,hydro}$
Ind	1979	2.4×10^7	1979	2.4×10^7
FAST	778	1.7×10^7	2022	2.4×10^7

a single SN in a self-gravitating gas cloud. When we take the mass of 10^6 $M_\odot$ and the radius of 100 pc as typical values of a giant molecular cloud (Dame et al. 1986), its potential energy is $\sim 10^{51}$ ergs (here we assume the cloud is in a virial equilibrium state). This value is comparable to the energy released by a single Type II SN. Therefore, in order to investigate the behavior of an exploding cloud induced by SN, we solved the evolution of a gas cloud with a positive total energy comparable to the absolute value of the original total energy.

We used the particle distribution of the three-dimensional collapse test at $T=3$ as the initial particle distribution of this explosion test. We added the thermal energy in the central 32 particles with SPH manner. Since the original total energy of the system is ~ -0.6, the new total energy of the system was set to be $E=0.5, 1, 2$, and 10. We set T to zero before the first step of the explosion calculation and follow the evolution to $T=5$. In this test, we also plot the results of the global time-step case.

Figure 5 shows snapshots of the expanding cloud, for the case of $E=2$, obtained with the FAST method at six different epochs ($T=0, 1, 2, 3, 4$ and 5). The particles in the region $|z|<0.1$ are shown in this figure. The initially compact gas cloud expands driven by the high pressure gas added in the center of the cloud, and forms a spherical shell-like structure. The shell moves outward, and at the final phase ($T=5$), the radius of the shell becomes ~ 5.

Figure 6 shows time evolutions of density peaks for simulations with several different values of the injection energy. The positions of peaks are derived by averaging the positions of the 10 particles with highest local density. For the reference, in this figure, we plotted the results obtained with the global-step method. There are good agreements between individual time-steps with/without FAST runs and the global time-step runs. This is because we adopted the time-step limiter for hydrodynamics (Saitoh & Makino 2009). Without this limiter, we would have failed to obtain agreements between different methods. The difference of the the positions between individual time-steps with/without FAST runs are summarized in table 4. $R_{\rm Ind}$ and $R_{\rm FAST}$ represent radii of shells at $T=5$ for individual time-step without/with FAST and global time-step runs, respectively. In this table, we also show the difference between $R_{\rm FAST}$ and $R_{\rm Global}$, which is the radius of the shell at $T=5$ for the global time-step runs. The difference between FAST and Ind is comparable or smaller than the difference for the result of global time-step.

Table 5 shows the timing results for the explosion test. We can see that the reduction in the cost of gravity calculation is much larger than that in the collapse test, and the reduction in the cost of tree construction is even larger. For $E=10$, reduction in the tree construction cost is a factor of eight.

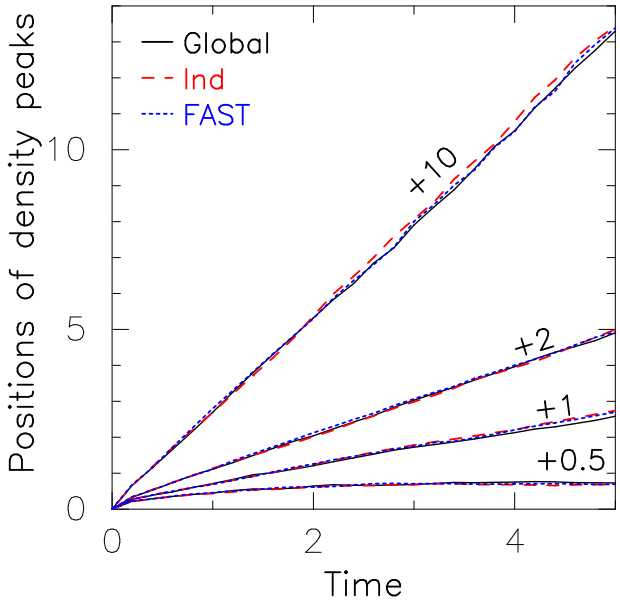

Fig. 6. Positions of density peaks as a function of time for various total energy cases. Solid, dashed, and dotted lines indicate evolutions of density peaks for cases of the global time-step (Global), ordinary individual time-steps (Ind), and individual time-steps with FAST (FAST). Numbers just above the lines indicate the values of the total energy.

Table 5. Timing results for cloud explosion tests.

		Time [sec]			
Method	E	Total	Gravity[a]	Hydro	Others
Ind	0.5	1264	498 (138)	550	216
FAST	0.5	972	175 (16)	568	229
Ind	1	1034	396 (100)	458	180
FAST	1	799	135 (15)	482	182
Ind	2	941	358 (92)	438	145
FAST	2	719	112 (14)	451	156
Ind	10	1018	383 (106)	466	169
FAST	10	758	89 (13)	484	185

[a] Items are the same as table 3.

The number of integrated particles and steps are summarized in table 6. By using the FAST method, we can greatly reduce steps for the gravity part. In these simulations, the use of the FAST method resulted in the reduction of the number of gravity steps by a factor of 7 to 9. The numbers of integrated particles for the gravity part are reduced to only $0.5-0.7$ times that of Ind runs. As is shown above, the speed up factors for the gravity part are $2.8-4.3$. These results indicate that the decrease of the number of steps is quite efficient for integrations of self-gravitating fluid. There is almost no change in the hydrodynamics part.

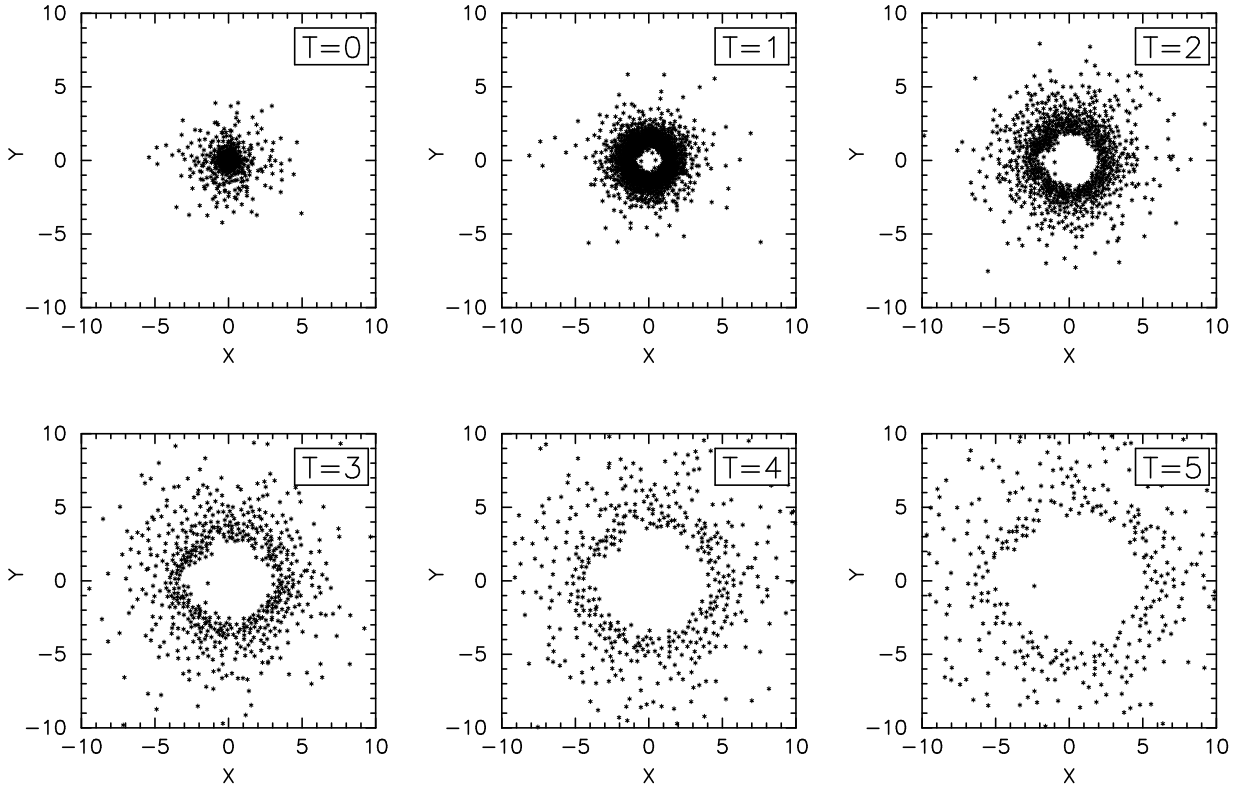

Fig. 5. Snapshots of the expanding cloud at six different epochs ($T = 0, 1, 2, 3, 4$ and 5). Projected particle distributions in a thin ($|z| < 0.1$) region are shown. Dots indicate projected particle positions. This is the case that the explosion simulation with $E = 2$. The time-integration was done by the individual time-steps with the FAST method.

Table 4. Differences between the peak positions with individual time-step with FAST and others (individual time-step without FAST and global time-step).

	$E = 0.05$	$E = 0.1$	$E = 0.2$	$E = 10$
$\left\|\frac{R_{\rm FAST}-R_{\rm Ind}}{R_{\rm Ind}}\right\|$	1.5 %	1.6 %	1.3 %	0.4 %
$\left\|\frac{R_{\rm FAST}-R_{\rm Global}}{R_{\rm Global}}\right\|$	6.4 %	6.2 %	1.9 %	1.1 %

Table 6. Steps and number of integrated particles for cloud explosion tests.

		Gravity		Hydro	
Method	E	steps	$N_{\rm int,grav}$	steps	$N_{\rm int,hydro}$
Ind	0.5	4675	9.0×10^6	4675	9.0×10^6
FAST	0.5	525	5.9×10^6	4431	8.8×10^6
Ind	1	3480	7.8×10^6	3480	7.8×10^6
FAST	1	479	4.8×10^6	3535	7.8×10^6
Ind	2	3515	7.5×10^6	3515	7.5×10^6
FAST	2	452	4.1×10^6	3397	7.4×10^6
Ind	10	3104	7.5×10^6	3104	7.5×10^6
FAST	10	427	3.4×10^6	3412	7.6×10^6

5.3. Test III: Merger simulations

In this section, we discuss the result of the application of the FAST method to a realistic problem, namely simulations of galaxy-galaxy collisions. Simulations we performed here were based on our recent galaxy-galaxy collision simulations of Saitoh et al. (2009), in which we followed the cooling of gas down to 10 K. We used the model of M1C. Gravity, hydrodynamics, radiative cooling, far-ultraviolet heating, star formation, and type-II SNe were taken into account. The condition for the star formation is that the gas is dense ($n_{\rm H} > 100$ cm^{-3}) and cold ($T < 100$ K) with converging flows. The regions which satisfy these conditions form stars following the Schmidt-law with the local star-formation efficiency of 0.033. Further details of the modeling of star formation were described in Saitoh et al. (2008) and Saitoh et al. (2009). Gravitational softening was set to be 20 pc for all particles. The initial numbers of dark matter, (old) star, and gas particles were 6930000, 341896, and 148104, respectively. We used 128 cores of Cray XT4 system at Center for Computational Astrophysics of National Astronomical Observatory of Japan.

Figure 7 shows density and temperature maps for merger simulations at $T = 420$ Myr by individual time-steps without and with the FAST method. We can easily

see that these two integration methods show quite similar results in density and temperature structures. The positions of "Heat spots" due to SNe are not perfectly identical because of run-to-run fluctuations. Other global properties of these galaxies are also identical for both runs.

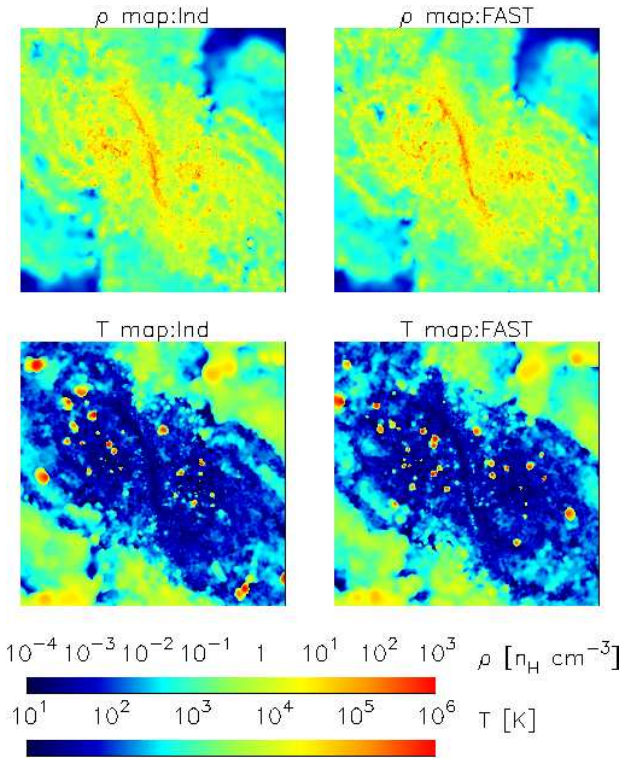

Fig. 7. Density and temperature maps for simulations by individual time-steps without and with the FAST method. Each panel shows 16 kpc × 16 kpc in the orbital plane. The left and right columns show the results by individual time-steps without and with the FAST method, respectively. The epoch of these maps is $T = 420$ Myr.

Figure 8 shows cumulative fractions of particles as a function of $dt_{\rm hydro}$ and $dt_{\rm grav}$ for SPH particles and $dt_{\rm nbody}$ for collisionless particles. The minimum time-step for the hydrodynamics part is shorter than that for the gravity part for SPH particles by a factor of eight. In addition, collisionless particles have longer time-steps than SPH particles. Therefore the gravity part is skipped in the lowest 3 levels and the calculation is accelerated significantly.

Table 7 shows timing results of merging simulations. We sampled two typical epochs, *i.e.*, 350 Myr $\leq T <$ 400 Myr and 400 Myr $\leq T <$ 450 Myr. The former epoch is a quiescent star forming phase before the first encounter while the later epoch is a significantly enhanced star forming phase during the first encounter. The total integration time for the simulation with the FAST method decreases by almost a factor of two from that of the simulation without the FAST method. With the FAST method, the gravity part is ~ 7 times faster than that without the FAST method. The reduction of the total calculation time is similar for quiescent and starburst phases.

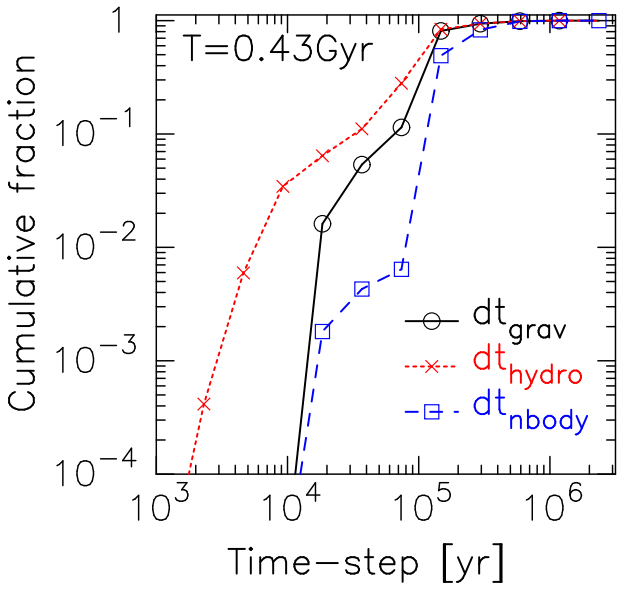

Fig. 8. Cumulative fractions of particles as a function of $dt_{\rm hydro}$ and $dt_{\rm grav}$ for SPH particles and $dt_{\rm nbody}$ for collisionless particles. The time-steps are sampled from the merger simulation by the individual time-step with FAST. The epoch is $T = 0.43$ Gyr. Solid, dotted, and dashed histograms indicate cumulative fractions of $dt_{\rm grav}$ and $dt_{\rm hydro}$ for SPH particles and $dt_{\rm nbody}$ for collisionless particles.

In table 8, we show numbers of time-steps and integrated particles for gravity and hydrodynamics parts. The simulation with the FAST method required ~ 7 times smaller number of gravity steps than that without the FAST method. Note that the number of integrated particles for gravity is almost the same for the Ind and FAST method. The large reduction in the calculation time is due to both the reduction of the number of tree constructions and the removal of force calculations with small number of particles, where the calculation becomes inefficient in individual time-steps or parallel computers.

6. Maximum Acceleration Factor by FAST

In this section, we estimate the maximum acceleration factor due to the introduction of the FAST method using a simple calculation cost model. By comparing the calculation costs of the runs with/without FAST, we obtain the acceleration factor due to the FAST method.

We here model the calculation cost of a simulation as follow:

$$t_{\rm all} = N_{\rm s,g}(t_{\rm t,g} + \tilde{N}_{\rm u,g} t_{\rm e,g}) + N_{\rm s,h}(t_{\rm t,h} + \tilde{N}_{\rm u,h} t_{\rm e,h}), \quad (29)$$

$$= N_{\rm s,g} t_{\rm grav} + N_{\rm s,h} t_{\rm hydro}. \quad (30)$$

where $N_{\rm s,g}$ and $N_{\rm s,h}$ are the number of steps for gravity and hydrodynamics, $t_{\rm t,g}$ and $t_{\rm t,h}$ are the calculation times of tree construction for gravity and hydrodynamics, $\tilde{N}_{\rm u,g}$ and $\tilde{N}_{\rm u,h}$ are the mean number of updated particles for gravity and hydrodynamics in each step, $t_{\rm e,g}$ and $t_{\rm e,h}$ are the mean evaluation time of gravity and hydrodynamical interactions for a single particle, respectively,

Table 7. Timing results for merger simulations.

		Time [sec]			
Method	Epoch	Total	Gravity[a]	Hydro	Others[b]
Ind	350 Myr → 400 Myr	14301	5887 (2132)	3545	4869
FAST	350 Myr → 400 Myr	7249	919 (264)	2923	3407
Ind	400 Myr → 450 Myr	16454	6703 (2441)	4041	5710
FAST	400 Myr → 450 Myr	9646	953 (279)	4152	4541

[a] Items are the same as table 3. [b] In this test runs, "Others" includes the calculation times of the radiative cooling, star formation, and SNe routines.

Table 8. Steps and number of integrated particles for merger simulations.

		Gravity		Hydro	
Method	Epoch	steps	$N_{\rm int,grav}$	steps	$N_{\rm int,hydro}$
Ind	350 Myr → 400 Myr	18697	1.6×10^9	18697	5.8×10^7
FAST	350 Myr → 400 Myr	2310	1.6×10^9	16626	6.4×10^7
Ind	400 Myr → 450 Myr	21296	1.8×10^9	21296	7.3×10^7
FAST	400 Myr → 450 Myr	2425	1.8×10^9	22959	8.0×10^7

and $t_{\rm grav}$ and $t_{\rm hydro}$ are the mean calculation times in a single step for gravity and hydrodynamics, respectively. In this model, we neglected the calculation cost of miscellaneous operations, such as domain decomposition, time-integration, evaluations of time-steps.

In traditional individual time-steps, the number of gravity steps is the same as that of hydrodynamical steps. Therefore the total calculation cost with traditional individual time-steps is

$$t_{\rm all,Ind} = N_{\rm s,h,Ind}(t_{\rm grav,Ind} + t_{\rm hydro,Ind}). \quad (31)$$

On the other hand, in FAST, the number of gravity steps is different from that of hydrodynamical steps. According to the argument in section 2, the number of hydrodynamical steps is about ten times larger than the gravity steps. It means $N_{\rm s,h,FAST} = 10 \times N_{\rm s,g,FAST}$ in equation (30). Thus, the total calculation cost with FAST expresses as

$$t_{\rm all,FAST} = N_{\rm s,h,FAST}(\frac{1}{10} t_{\rm grav,FAST} + t_{\rm hydro,FAST}). \quad (32)$$

The acceleration factor is defined as $\tau = t_{\rm all,Ind}/t_{\rm all,FAST}$. If we assume that the number of hydrodynamical steps in the calculation without FAST is the same as that with FAST and that calculation times between with/without FAST are the same, the acceleration factor is

$$\tau = \frac{10(t_{\rm grav} + t_{\rm hydro})}{t_{\rm grav} + 10 t_{\rm hydro}}. \quad (33)$$

In this equation, we removed suffixes Ind and FAST of calculation costs. Here we consider three typical cases that $t_{\rm grav} \gg t_{\rm hydro}$, $t_{\rm grav} = t_{\rm hydro}$, and $t_{\rm grav} \ll t_{\rm hydro}$. The first case corresponds to usual N-body/SPH simulations. In this case, the acceleration factor is $\tau = 10$, and is quite large. The second case corresponds to the case that (a) the calculation time of the gravitational force reduces significantly by adopting hardware/software accelerators, such as GRAPE or Phantom-GRAPE, and/or (b) the calculation cost of hydrodynamics is rather expensive because of the treatment of complex baryon physics, for instance star formation, SNe, and chemical evolution. The acceleration factor in this case is $\tau \sim 2$. Our simulations are close to the second case. The final case is the ideal case that the calculation cost for gravity is negligible. In this case, the acceleration factor becomes unity and the gain due to FAST is zero. We do not think this hypothetical situation can occur.

7. Summary

In this paper, we describe a fast integrated method, "FAST" for self-gravitating fluid. The FAST method assigns different time-steps for gravitational and hydrodynamical interactions and integrates them asynchronously. The formulation of the FAST method is similar to the multi time-step method (Streett et al. 1978) and also regarded as an extension of "multi-step" symplectic integrators, such as mixed variable symplectic (Wisdom & Holman 1991), multiple stepsize (Skeel & Biesiadecki 1994), and the BRIDGE (Fujii et al. 2007) methods.

The approach of the FAST method is qualitatively different from other reduction techniques of the tree construction in gravity part. Thus the FAST method eliminates unnecessary tree constructions and gravity calculations by adopting longer time-steps for gravitational evolution than that for hydrodynamics.

We found that the evolution of collapsing and exploding self-gravitating fluid by the FAST method are identical to these by the usual unsplit method which integrates gravity and hydrodynamics synchronously.

As a realistic test, we applied the FAST method to merger simulations including self-gravity, hydrodynamics, radiative cooling, far-ultraviolet heating, and SN (Saitoh et al. 2009). In this test, we found that simulations with

and without the FAST method showed quite similar evolution. The calculation with FAST was nearly a factor of two faster. This large gain was due to the reduction in the gravity steps with small number of particles. The FAST method is very effective in accelerating simulations of self-gravitating fluid.

We thank the anonymous referee for his/her insightful comments and suggestions, which helped us to greatly improve our manuscript. We also thank Takashi Ito, Keiichi Wada, Michiko Fujii and Tomoaki Ishiyama for useful discussion and Kohji Yoshikawa, who kindly provided us with a custom version of the Phantom-GRAPE library. A part of numerical tests were carried out on Cray XT4 and GRAPE system at Center for Computational Astrophysics of National Astronomical Observatory of Japan. This project is supported by Grant-in-Aid for Scientific Research (17340059) of JSPS, MEXT Japan the Special Coordination Fund for Promoting Science and Technology, "GRAPE-DR Project", and Molecular-Based New Computational Science Program of NINS. TRS is financially supported by a Research Fellowship from the Japan Society for the Promotion of Science for Young Scientists.

Appendix 1. Symplectic integration method and its variants

In this appendix, we explain the symplectic integration method briefly. Then we explain sophisticated versions of symplectic integration methods, *i.e.*, mixed variable symplectic method (Wisdom & Holman 1991), multiple stepsize method (Skeel & Biesiadecki 1994), and the BRIDGE (Fujii et al. 2007) methods.

Symplectic integration methods (e.g., Dragt & Finn 1976; Forest & Ruth 1990; Yoshida 1990; Yoshida 1993) are now widely used in the simulations of gravitating N-body systems. These methods preserve the symplectic form of the canonical equation of motions when calculating the time variation of the system. This character leads to the very good conservation of system's total energy on the course of numerical calculation.

When we express H as the Hamiltonian of the system, and p and q as six-dimension coordinates, canonical equations are

$$\frac{dq}{dt} = \frac{\partial H}{\partial p}, \tag{A1}$$

$$\frac{dp}{dt} = -\frac{\partial H}{\partial q}. \tag{A2}$$

We can summarize above two equations as

$$\frac{df}{dt} = \{f, H\}, \tag{A3}$$

where f is p or q, respectively, and $\{,\}$ is a Poisson bracket. We define an operator that

$$\{, H\}f \equiv \{f, H\}. \tag{A4}$$

We can write a generalized canonical equation (A3) as

$$\frac{df}{dt} = \{, H\}f. \tag{A5}$$

When we integrate equation (A5) from t to $t + \Delta t$, the formal solution of the equation (A5) is written as

$$f(t + \Delta t) = e^{\Delta t\{, H\}} f(t). \tag{A6}$$

Here, we consider the Hamiltonian of a self-gravitating system with N particles. In this case, the Hamiltonian is written as

$$H = H_{\rm A} + H_{\rm B}, \tag{A7}$$

where

$$H_{\rm A} = \sum_{i}^{N} \frac{p_i^2}{2m_i}, \tag{A8}$$

$$H_{\rm B} = -\sum_{i<j}^{N} \frac{G m_i m_j}{q_{ij}}. \tag{A9}$$

The formal solution is written as

$$f(t + \Delta t) = e^{\Delta t(\{, H_{\rm A}\} + \{, H_{\rm B}\})} f(t). \tag{A10}$$

Applying Barker-Champbell-Hausdorff formula (Varadarajan 1984) to equation (A10), we obtain a first order integrator

$$f(t + \Delta t) \approx e^{\Delta t\{, H_{\rm A}\}} e^{\Delta t\{, H_{\rm B}\}} f(t), \tag{A11}$$

and a second order integrator

$$f(t + \Delta t) \approx e^{\frac{\Delta t}{2}\{, H_{\rm B}\}} e^{\Delta t\{, H_{\rm A}\}} e^{\frac{\Delta t}{2}\{, H_{\rm B}\}} f(t). \tag{A12}$$

This second order integrator is well known as the *leap-frog* integrator.

It is widely known that symplectic integration methods can achieve high-accuracy once we split Hamiltonians into several components. Mixed variable symplectic (MVS) method (Wisdom & Holman 1991; Kinoshita et al. 1991) splits the Hamiltonian into an unperturbed part with an analytic solution (i.e., Keplerian motion when we traced planetary motion) and a perturbation part (i.e., mutual gravitational perturbation among planets). When the system is nearly integrable, the Hamiltonian for the unperturbed part becomes much larger than that of the perturbed part, which enables the method to accomplish a very high accuracy in integrating the equations of motion, compared with conventional symplectic integrators.

The multiple stepsize (MSS) method (Skeel & Biesiadecki 1994; Duncan et al. 1998) splits a potential into the sum of potentials of a short-range and a long-range forces and gives different time-steps for different ranges of forces. The MSS method accomplishes the similar accuracy compared with the usual symplectic method applied with small time-step. The use of different time-steps for different interactions was proposed for the integration of molecular dynamics (Streett et al. 1978). `GADGET-2` (Springel 2005), which employs a TreePM method for gravitational force calculation, adopts different time-steps for the long-range force derived from

a Particle-mesh method (Hockney & Eastwood 1981) and the short-range force derived from a Tree method (Barnes & Hut 1986).

BRIDGE (Fujii et al. 2007) was developed in order to solve galaxy-star cluster systems self-consistently. BRIDGE divides a Hamiltonian of a galaxy-star cluster system into a star cluster and a galaxy parts, and applies different time-steps and integrators. In BRIDGE, the integration of star cluster particles is performed by a forth-order integration method, namely Hermit method (Makino & Aarseth 1992). Force calculations among star clusters are performed by direct method with GRAPE (Sugimoto et al. 1990). The integration of galaxy particles is performed by the leap-frog method with the Tree method for the force estimation. Forces between star cluster particles and galaxy particles are also calculated by the Tree method with constant time-step. Therefore this method can deal with coevolution of collisionless and collisional systems self-consistently.

References

Aarseth, S. J. 1963, MNRAS, 126, 223
Barnes, J., & Hut, P. 1986, Nature, 324, 446
Dame, T. M., Elmegreen, B. G., Cohen, R. S., & Thaddeus, P. 1986, ApJ, 305, 892
Dragt, A. J., & Finn, J. M. 1976, Journal of Mathematical Physics, 17, 2215
Duncan, M. J., Levison, H. F., & Lee, M. H. 1998, AJ, 116, 2067
Evrard, A. E. 1988, MNRAS, 235, 911
Farr, W. M., & Bertschinger, E. 2007, ApJ, 663, 1420
Forest, E., & Ruth, R. D. 1990, Phys. D, 43, 105
Fujii, M., Iwasawa, M., Funato, Y., & Makino, J. 2007, PASJ, 59, 1095
Gerritsen, J. P. E. 1997, PhD thesis, , Groningen University, the Netherlands, (1997)
Gingold, R. A., & Monaghan, J. J. 1977, MNRAS, 181, 375
Governato, F. et al. 2009, MNRAS, 957
Hernquist, L., & Katz, N. 1989, ApJS, 70, 419
Heyer, M. H., & Brunt, C. M. 2004, ApJL, 615, L45
Hockney, R. W., & Eastwood, J. W. 1981, Computer Simulation Using Particles (Computer Simulation Using Particles, New York: McGraw-Hill, 1981)
Ito, T., Ebisuzaki, T., Makino, J., & Sugimoto, D. 1991, PASJ, 43, 547
Katz, N., & Gunn, J. E. 1991, ApJ, 377, 365
Kawai, A., Fukushige, T., Makino, J., & Taiji, M. 2000, PASJ, 52, 659
Kim, J., Park, C., Gott, J. R., & Dubinski, J. 2009, ApJ, 701, 1547
Kinoshita, H., Yoshida, H., & Nakai, H. 1991, Celestial Mechanics and Dynamical Astronomy, 50, 59
Larson, R. B. 1981, MNRAS, 194, 809
Lucy, L. B. 1977, AJ, 82, 1013
Makino, J. 1991a, PASJ, 43, 859
—. 1991b, PASJ, 43, 621
Makino, J., & Aarseth, S. J. 1992, PASJ, 44, 141
Makino, J., Fukushige, T., Koga, M., & Namura, K. 2003, PASJ, 55, 1163
Makino, J., Hut, P., Kaplan, M., & Saygın, H. 2006, New Astronomy, 12, 124
Makino, J., Taiji, M., Ebisuzaki, T., & Sugimoto, D. 1997, ApJ, 480, 432
McMillan, S. L. W. 1986, in Lecture Notes in Physics, Berlin Springer Verlag, Vol. 267, The Use of Supercomputers in Stellar Dynamics, ed. P. Hut & S. L. W. McMillan, 156–+
McMillan, S. L. W., & Aarseth, S. J. 1993, ApJ, 414, 200
Monaghan, J. J. 1992, ARA&A, 30, 543
—. 1997, Journal of Computational Physics, 136, 298
Navarro, J. F., & Benz, W. 1991, ApJ, 380, 320
Nelson, A. F., Wetzstein, M., & Naab, T. 2009, ApJS, 184, 326
Okamoto, T., Nemmen, R. S., & Bower, R. G. 2008, MNRAS, 385, 161
Okumura, S. K. et al. 1993, PASJ, 45, 329
Saitoh, T. R., Daisaka, H., Kokubo, E., Makino, J., Okamoto, T., Tomisaka, K., Wada, K., & Yoshida, N. 2008, PASJ, 60, 667
—. 2009, PASJ, 61, 481
Saitoh, T. R., & Makino, J. 2009, ApJL, 697, L99
Salpeter, E. E. 1955, ApJ, 121, 161
Skeel, R. D., & Biesiadecki, J. J. 1994, Ann. Numer. Math, 1, 191
Solomon, P. M., Rivolo, A. R., Barrett, J., & Yahil, A. 1987, ApJ, 319, 730
Springel, V. 2005, MNRAS, 364, 1105
Springel, V., Yoshida, N., & White, S. D. M. 2001, New Astronomy, 6, 79
Steinmetz, M., & Mueller, E. 1993, A&A, 268, 391
Stinson, G., Seth, A., Katz, N., Wadsley, J., Governato, F., & Quinn, T. 2006, MNRAS, 373, 1074
Streett, W. B., Tildesley, D. J., & Saville, G. 1978, Molecular Physics, 35, 639
Sugimoto, D., Chikada, Y., Makino, J., Ito, T., Ebisuzaki, T., & Umemura, M. 1990, Nature, 345, 33
Suto, Y., & Suginohara, T. 1991, ApJL, 370, L15
Thacker, R. J., & Couchman, H. M. P. 2000, ApJ, 545, 728
Varadarajan, V. 1984, Lie Groups, Lie Algebras and their Representations (Springer, Berlin)
Wadsley, J. W., Stadel, J., & Quinn, T. 2004, New Astronomy, 9, 137
Wetzstein, M., Nelson, A. F., Naab, T., & Burkert, A. 2009, ApJS, 184, 298
Wisdom, J., & Holman, M. 1991, AJ, 102, 1528
Yoshida, H. 1990, Physics Letters A, 150, 262
—. 1993, Celestial Mechanics and Dynamical Astronomy, 56, 27